

Electric-field-induced fully-compensated ferrimagnetism in experimentally synthesized monolayer MnSe

Liguo Zhang and San-Dong Guo*

School of Electronic Engineering, Xi'an University of Posts and Telecommunications, Xi'an 710121, China

Gangqiang Zhu

School of Physics and Electronic Information, Shaanxi Normal University, Xi'an 716000, Shaanxi, China

Owing to their inherent characteristics of zero stray field and terahertz dynamics, two-dimensional (2D) zero-net-magnetization magnets demonstrate the potential for miniaturization, ultradensity and ultrafast performance. Recently, fully-compensated ferrimagnet of 2D zero-net-magnetization magnets has already attracted attention, as it can exhibit global spin-splitting, magneto-optical response and anomalous Hall effect [Phys. Rev. Lett. 134, 116703 (2025)]. Therefore, it is very important to provide experimentally feasible strategies and materials to achieve fully-compensated ferrimagnets. Here, we use the experimentally synthesized A-type PT -antiferromagnet (the joint symmetry (PT) of space inversion symmetry (P) and time-reversal symmetry (T)) MnSe as the parent material to induce fully-compensated ferrimagnetism through an out-of-plane electric field. This electric field can remove the P symmetry of the lattice, thereby breaking the PT symmetry and inducing spin-splitting. When considering spin-orbital coupling (SOC), MnSe with an out-of-plane magnetization can achieve the anomalous valley Hall effect (AVHE). In addition, we also discuss inducing fully-compensated ferromagnetism via Se vacancies and Janus engineering. Our works can promote the further development of 2D fully-compensated ferrimagnets both theoretically and experimentally.

Magnetism is pivotal in driving technological advancements. Ferromagnets have been the focus of intensive research and have found widespread applications across various fields[1]. Compared with ferromagnets, zero-net-magnetization magnets offer more advantages for spintronic devices[2, 3]. They enable high storage density, robustness against external magnetic fields, and ultrafast writing speeds, all thanks to their zero-net magnetic moment. From a symmetric perspective, the collinear magnets with zero-net-magnetization primarily consist of PT -antiferromagnets (the joint symmetry (PT) of space inversion symmetry (P) and time-reversal symmetry (T)), alternemagnets, and fully-compensated ferrimagnets[4, 5].

For PT -antiferromagnets, the energy bands are spin-degenerate throughout the entire Brillouin zone (BZ) ($E_{\uparrow}(k)=PTE_{\uparrow}(k)=E_{\downarrow}(k)$), which prevents many interesting physical effects, such as magneto-optical effect, anomalous Hall effect and anomalous valley Hall effect (AVHE)[6, 7]. For alternemagnets, the real-space magnetic order closely resembles that of a collinear antiferromagnet, characterized by a perfectly spin-compensated arrangement. However, in the momentum space, the spin-splitting represents a natural extension of ferromagnetism, featuring non-relativistic spin-split bands with d -wave, g -wave or i -wave symmetry[4, 5]. Alternemagnets have exhibited a range of phenomena that are previously deemed exclusive to ferromagnets. These phenomena include non-relativistic lifted Kramers degeneracy, anomalous Hall/Nernst effect, non-relativistic spin (polarized) currents, and magneto-optical Kerr effect[6].

Fully-compensated ferrimagnets represent a unique

class of ferrimagnetic materials, characterized by their zero-net magnetization[8–10]. The spin-splitting in these materials occurs throughout the entire BZ with s -wave symmetry, resembling the behavior observed in ferromagnets. Similar to alternemagnet, fully-compensated ferrimagnet can also show anomalous Hall/Nernst effect, non-relativistic spin (polarized) currents, and magneto-optical Kerr effect. Recently, the importance of two-dimensional (2D) fully-compensated ferrimagnetism has gained increasing recognition, thereby expanding the domain of low-dimensional spintronic materials[11]. Hence, it is crucial to develop experimentally viable strategies and materials for the realization of 2D fully-compensated ferrimagnets. From the perspective of symmetry, fully-compensated ferrimagnet can be obtained by breaking the inversion symmetry of PT -antiferromagnet and the rotational or mirror symmetry of alternemagnet.

A monolayer of MnSe, combined with an AA-stacked bilayer silicene crystal lattice and exhibiting A-type antiferromagnetic (AFM) ordering, has recently been successfully synthesized experimentally[12]. MnSe is a typical PT -antiferromagnet. Here, we use an out-of-plane electric field to break the PT symmetry of MnSe, thereby achieving fully-compensated ferrimagnetism. Very recently, fully-compensated ferrimagnetism has been experimentally realized in bilayer CrPS₄ by a perpendicular electric field, which can switch the spin polarization of the conduction band on and off[13]. This further confirms the feasibility of our proposal. The electric field, in conjunction with the spin-orbital coupling (SOC), has the potential to enable MnSe to exhibit AVHE. Additionally, we explore the induction of fully-compensated ferromag-

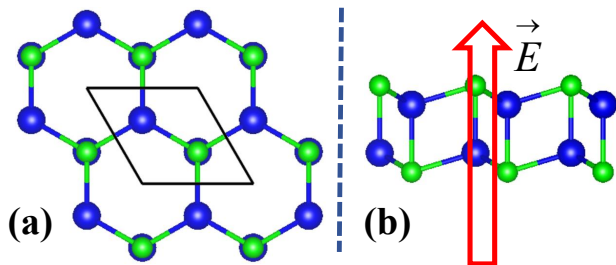


FIG. 1. (Color online) For monolayer MnSe, the top (a) and side (b) views of crystal structures. In (a, b), the blue and green balls represent Mn and Se atoms, respectively. In (b), the red arrow represents the out-of-plane electric field.

netism through Se vacancies and Janus engineering.

We conduct spin-polarized first-principles calculations within density functional theory (DFT)[14] using the Vienna Ab Initio Simulation Package (VASP)[15–17]. The Perdew-Burke-Ernzerhof generalized gradient approximation (PBE-GGA)[18] is employed as the exchange-correlation functional. The calculations are performed with the kinetic energy cutoff of 500 eV, total energy convergence criterion of 10^{-8} eV, and force convergence criterion of $0.001 \text{ eV} \cdot \text{\AA}^{-1}$. To account for the localized nature of Mn- $3d$ orbitals, a Hubbard correction $U_{eff}=2.3 \text{ eV}$ [12] is applied using the rotationally invariant approach proposed by Dudarev et al[19]. A vacuum space of more than 15 \AA along the z -direction is introduced to prevent interactions between neighboring slabs. The BZ is sampled using a $15 \times 15 \times 1$ Monkhorst-Pack k -point meshes for crystal structure optimization and electronic structure calculations. The Berry curvatures are calculated directly from the wave functions using Fukui’s method[20], as implemented in the VASP-BERRY code[21–23].

The monolayer MnSe has been synthesized in experiment[12]. As shown in Figure 1, the MnSe monolayer includes two buckled honeycomb MnSe sublayers, and they are interconnected by Mn-Se bonds. MnSe monolayer crystallizes in the $P3m1$ (No. 164), with lattice P symmetry. It has been proved that the upper and lower sublayers are coupled antiferromagnetically through A-type AFM ordering[12]. The optimized equilibrium lattice constants are $a=b=4.27 \text{ \AA}$. When considering magnetic ordering, MnSe monolayer possesses PT symmetry as a PT -antiferromagnet, giving rise to spin-degenerate energy bands.

In order to achieve fully-compensated ferrimagnet, PT symmetry of MnSe monolayer should be broken, and its total magnetic moment still remains zero. When an out-of-plane electric field is applied, the lattice P symmetry can be removed. In other words, an out-of-plane electric field can break the PT symmetry by generating layer-dependent electrostatic potential, giving rise to fully-compensated ferrimagnetism. Both sublayers of MnSe

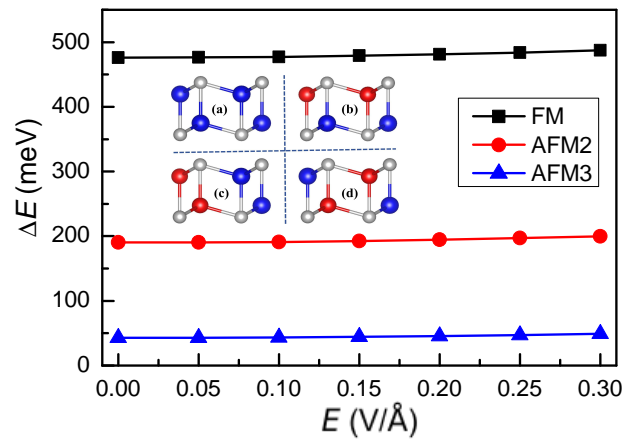


FIG. 2. (Color online) For MnSe, the energy difference between FM/AFM2/AFM3 and AFM1 orderings as a function of E (AFM1 ordering as a reference point). The inset shows four magnetic configurations, including FM (a), AFM1 (b), AFM2 (c) and AFM3 (d), and the blue, red and gray balls represent Mn_{up} , Mn_{dn} and Se atoms, respectively.

possess built-in electric fields, which are oriented in opposite directions and cancel each other out, resulting in a zero-net electric field. Therefore, by perturbing the built-in electric field of one sublayer through Se vacancies, the equilibrium is disrupted, and a net built-in electric field can be generated, leading to fully-compensated ferrimagnetism. In fact, the out-of-plane electric field can also be equivalently replaced by the built-in electric field achieved through Janus engineering, producing fully-compensated ferrimagnetism.

Electric field can be an effective tool to break the lattice P symmetry in 2D materials[24]. In order to achieve fully-compensated ferrimagnetism, magnetic ordering is another important factor. Therefore, we first determine the magnetic ground state of MnSe under the applied electric field. As plotted in Figure 2, four magnetic configurations, including FM, AFM1, AFM2 and AFM3 orderings, are considered, and AFM1 case of them is A-type AFM ordering. The differences in energy between ferromagnetic (FM), AFM2, AFM3 and AFM1 states as a function of electric field E are plotted in Figure 2. Within considering E range, MnSe monolayer always has AFM1 ordering, which provides the basic conditions to achieve fully-compensated ferrimagnetism. With the increasing electric field, all energy differences increase, which means that the electric field can enhance magnetic interactions.

The energy band structures of MnSe without SOC at representative $E=+0.0, +0.1, +0.2$ and $+0.3 \text{ V/\AA}$ are shown in Figure 3. Figure 3 (a) shows the band structure without an electric field. Due to PT symmetry, the spin-up and spin-down bands are degenerate throughout the whole BZ. It is an indirect band gap semiconductor with gap value of 1.80 eV , which agrees well with available value of 1.76 eV [25]. The magnetic moments (absolute

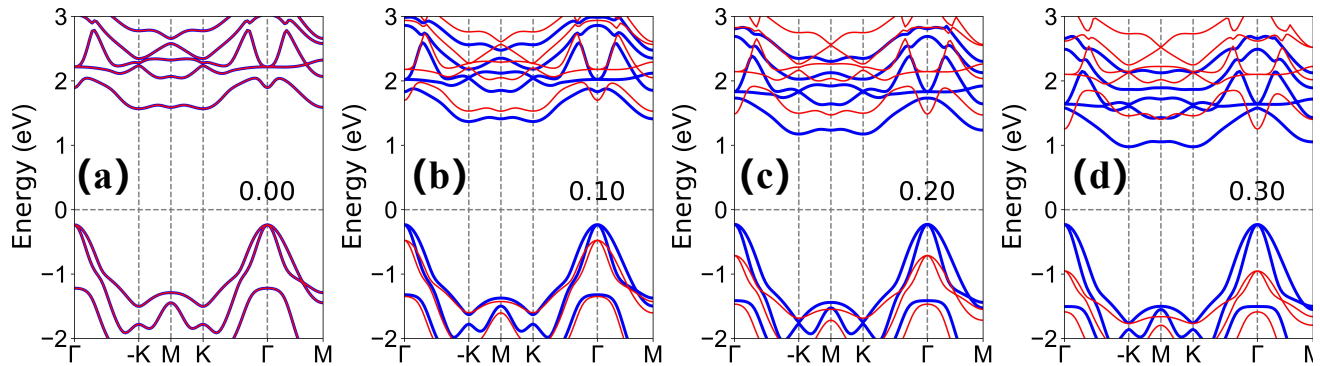


FIG. 3. (Color online) For MnSe, the energy band structures without SOC at representative $E=+0.0$ (a), $+0.1$ (b), $+0.2$ (c) and $+0.3$ (d) $\text{V}/\text{\AA}$. In (a, b, c, d), the blue (red) represents spin-up (spin-down) characters.

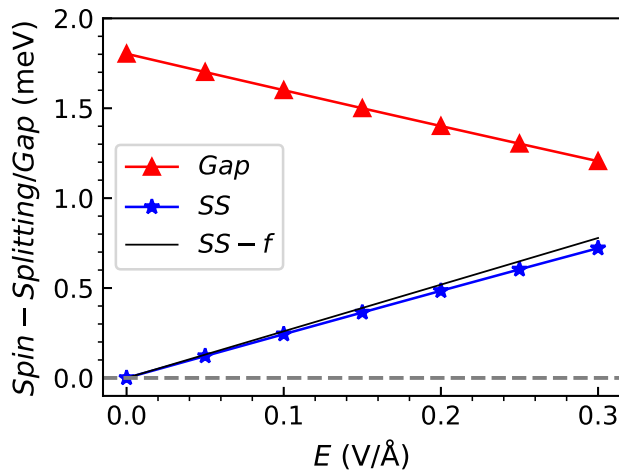


FIG. 4. (Color online) For MnSe, the spin-splitting (SS) between first/second and third/fourth valence bands at Γ point and energy bandgap (Gap) as a function of E . This black line ($SS - f$) represents the linear fitting through the eEd .

value) of Mn atoms of two sublayers are strictly equal due to lattice P symmetry, and they are $4.38 \mu_B$.

Upon the application of an out-of-plane electric field, a layer-dependent electrostatic potential is produced to break PT symmetry, and the spin degeneracy of the bands is lifted. At representative $E=+0.3 \text{ V}/\text{\AA}$, the magnetic moments of two Mn atoms are $-4.35 \mu_B$ and $4.38 \mu_B$, and their absolute values not strictly equal due to broken P symmetry. However, the total magnetic moment of MnSe is still equal to $0 \mu_B$ in the presence of an electric field (The sum of magnetic moments of Mn atom, Se atoms and interstitial region is zero.). This compensation is strict, which is not symmetry-driven, but rather due to the integer requirement of the magnetic moment caused by the energy gap[11]. Therefore, if the total magnetization of MnSe is zero under an applied electric field, it will be strictly zero. Electric field makes MnSe to be a fully-compensated ferrimagnet. When the direction of electric field is reversed, the order of spin splitting is also

reversed (See FIG.S1[26]).

The spin-splitting between first/second and third/fourth valence bands at Γ point and energy bandgap of MnSe as a function of E are plotted in Figure 4. With increasing E , the energy bandgap decreases linearly, while spin-splitting increases linearly. We also predict the spin-splitting by eEd [27], where e denotes the electron charge, and the d is the difference in the average z -values of Mn and Se atoms of two MnSe sublayers (about 2.594\AA). It is found that the estimated spin-splitting is very close to the first-principle result. At representative $E=+0.3 \text{ V}/\text{\AA}$, the spin-splitting can reach about 0.72 eV . Recently, an intense electric field larger than $0.4 \text{ V}/\text{\AA}$ has been achieved in 2D materials by dual ionic gating[28], which provides the possibility of achieving a fully-compensated ferrimagnet with large spin-splitting in MnSe.

For 2D zero-net-magnetization magnets, the fully-compensated ferrimagnet is a natural platform to realize the AVHE[7]. The orientation of magnetization plays a crucial role in generating spontaneous valley polarization. Specifically, only an out-of-plane magnetization direction can induce spontaneous valley splitting[7]. The magnetic orientation can be determined by calculating the magnetocrystalline anisotropy energy (MAE), which is given by the formula $E_{MAE} = E_{SOC}^{\parallel} - E_{SOC}^{\perp}$. Here, E_{SOC}^{\parallel} and E_{SOC}^{\perp} represent the energies when the spins are aligned in-plane and out-of-plane, respectively. The calculated MAE as a function of E are plotted in FIG.S2[26], and the negative value indicates the in-plane magnetization of MnSe within considered E range.

At $E=+0.3 \text{ V}/\text{\AA}$, the energy band structures with in-plane magnetization are plotted Figure 5 (a), which shows no valley splitting. To achieve valley polarization, the in-plane magnetization should be tuned into out-of-plane case. In experiment, the manipulation of the Néel vector can be effectively achieved through the application of spin-orbit torques (SOTs). Notably, experimental efforts have realized the reorientation of Néel vectors with switching angles of 90° , 120° or 180° [29].

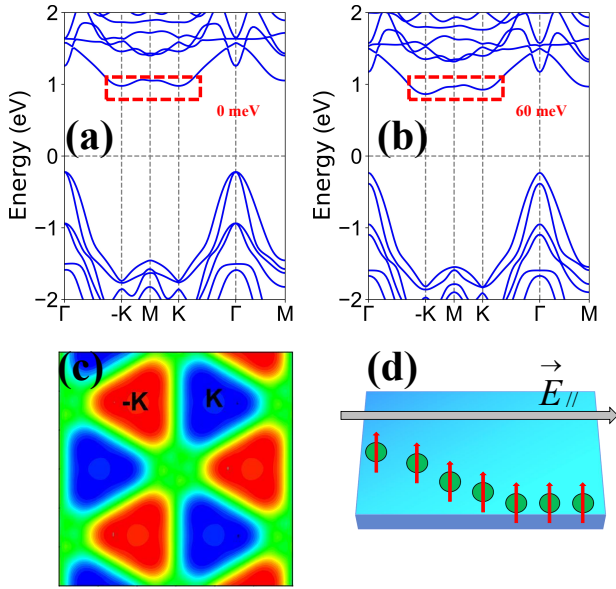


FIG. 5. (Color online) For MnSe at $E = +0.3 \text{ V/\AA}$, (a and b): the energy band structures within SOC, including in-plane (a) and out-of-plane (b) magnetization directions; (c): for (b) case, the distribution of Berry curvatures of spin-up; (d): for (b) case, an appropriate doping can produce AVHE in the presence of a longitudinal in-plane electric field (gray arrow).

At $E = +0.3 \text{ V/\AA}$, the energy band structures with out-of-plane magnetization are shown in Figure 5 (b). The valley polarization with the valley splitting of 60 meV ($\Delta E_C = E_K^C - E_{-K}^C$) can be achieved in the conduction bands, and the energy of K valley is higher than one of -K valley.

The -K and K valleys originate from the spin-up channel. The distribution of Berry curvatures for spin-up is depicted in Figure 5 (c). It is evident that the Berry curvatures are opposite for the -K and K valleys. Upon applying a longitudinal in-plane electric field, the Bloch carriers acquire an anomalous transverse velocity $v_{\perp} \sim E_{\parallel} \times \Omega(k)$ [30]. When the Fermi level is positioned between the -K and K valleys of the conduction band, only the spin-up electrons in the -K valley migrate to the boundary of the sample under the influence of an in-plane electric field, as shown in Figure 5 (d), which gives rise to AVHE[31].

In addition to the external electric field, vacancies may induce fully-compensated ferrimagnetism in MnSe. To simulate vacancies, we construct a 2×2 supercell, in which one quarter of the Se atoms in upper sublayer are replaced by vacancies (see Figure 6 (a)). Calculated results show that the total magnetic moment of MnSe with Se-vacancy is still equal to $0 \mu_B$, and its band structure shows significant spin-splitting (see Figure 6 (c)). These imply that vacancy can indeed transform MnSe into a fully-compensated ferrimagnet.

In fact, the external electric field can be equiva-

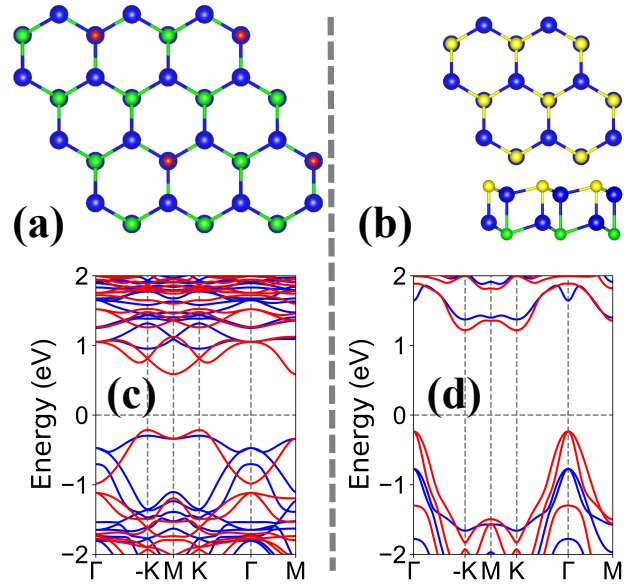


FIG. 6. (Color online) (a and b): the crystal structures of Se-vacancy MnSe and Janus Mn_2SSe along with their energy band structures (c and d) without SOC. In (a, b), the blue, green, yellow and red balls represent Mn atoms, Se atoms, S atoms and Se vacancies, respectively. In (c, d), the blue (red) represents spin-up (spin-down) characters.

lently replaced by the built-in electric field, which can be achieved through Janus engineering. The Janus Mn_2SSe and Mn_2SeTe have been predicted to possess A-type AFM ordering with good dynamic and thermal stabilities[25], and the crystal structures of Mn_2SSe are plotted in Figure 6 (b). Janus monolayer crystallizes in the $P3m1$ (No. 156), and the lack of horizontal mirror symmetry induces a built-in electric field. The energy band structures of Janus $\text{Mn}_2\text{SSe}/\text{Mn}_2\text{SeTe}$ are plotted in Figure 6 (d)/FIG.S3[26], which is similar to that of MnSe with external electric field, showing obvious spin-splitting. The net magnetic moment of Janus monolayers still remains zero. These show that Janus Mn_2SSe and Mn_2SeTe are fully-compensated ferrimagnets. When considering the SOC, Janus monolayers with out-of-plane magnetization can simultaneously exhibit valley-splitting (FIG.S4[26]) and spin-splitting (Figure 6 (d)), which can lead to the realization of AVHE.

In summary, we explore the potential of achieving fully-compensated ferrimagnetism based on the A-type PT -antiferromagnet MnSe as a parent material. By applying an out-of-plane electric field, the lattice P symmetry is removed, thereby breaking the PT symmetry and inducing spin-splitting. This manipulation, combined with SOC, enables MnSe to exhibit AVHE. Our findings provide experimentally feasible approaches to realizing fully-compensated ferrimagnets, thereby advancing the development of 2D magnetic materials with enhanced performance for miniaturization, ultradensity, and ultra-fast applications.

Conflicts of interest

There are no conflicts to declare.

This work is supported by Natural Science Basis Research Plan in Shaanxi Province of China (2021JM-456). We are grateful to Shanxi Supercomputing Center of China, and the calculations were performed on TianHe-2.

* sandongyuwang@163.com

- [1] S. A. Wolf, D. D. Awschalom, R. A. Buhrman, J. M. Daughton, S. von Molnár, M. L. Roukes, A. Y. Chtchelkanova and D. M. Treger, Spintronics: a spin-based electronics vision for the future, *Science* **294**, 1488 (2001).
- [2] X. Hu, Half-metallic antiferromagnet as a prospective material for spintronics, *Adv. Mater.* **24**, 294 (2012).
- [3] T. Jungwirth, J. Sinova, A. Manchon, X. Marti, J. Wunderlich and C. Felser, The multiple directions of antiferromagnetic spintronics, *Nat. Phys.* **14**, 200 (2018).
- [4] L. Šmejkal, J. Sinova and T. Jungwirth, Beyond conventional ferromagnetism and antiferromagnetism: A phase with nonrelativistic spin and crystal rotation symmetry, *Phys. Rev. X* **12**, 031042 (2022).
- [5] I. Mazin, Altermagnetism—a new punch line of fundamental magnetism, *Phys. Rev. X* **12**, 040002 (2022).
- [6] L. Bai, W. Feng, S. Liu, L. Šmejkal, Y. Mokrousov, and Y. Yao, Altermagnetism: Exploring New Frontiers in Magnetism and Spintronics, *Adv. Funct. Mater.* **34**, 2409327 (2024).
- [7] S. D. Guo, Valley polarization in two-dimensional zero-net-magnetization magnets, *Appl. Phys. Lett.* **126**, 080502 (2025).
- [8] H. van Leuken and R. A. de Groot, Half-Metallic Antiferromagnets, *Phys. Rev. Lett.* **74**, 1171 (1995).
- [9] H. Akai and M. Ogura, Half-Metallic Diluted Antiferromagnetic Semiconductors, *Phys. Rev. Lett.* **97**, 026401 (2006).
- [10] S. Wurmehl, H. C. Kandpal, G. H. Fecher, and C. Felser, Valence electron rules for prediction of half-metallic compensated-ferrimagnetic behaviour of Heusler compounds with complete spin polarization, *J. Phys.: Condens. Matter* **18**, 6171 (2006).
- [11] Y. Liu, S. D. Guo, Y. Li and C. C. Liu, Two-dimensional fully-compensated Ferrimagnetism, *Phys. Rev. Lett.* **134**, 116703 (2025).
- [12] M. Aapro, M. N. Huda, J. Karthikeyan, S. Kezilebieke, S. C. Ganguli, H. G. Herrero, X. Huang, P. Liljeroth and H.-P. Komsa, Synthesis and properties of monolayer MnSe with unusual atomic structure and antiferromagnetic ordering, *ACS Nano* **15**, 13794 (2021).
- [13] F. Yao, M. Liao, M. Gibertini et al., Switching on and off the spin polarization of the conduction band in antiferromagnetic bilayer transistors. *Nat. Nanotechnol.* (2025). <https://doi.org/10.1038/s41565-025-01872-w>
- [14] P. Hohenberg and W. Kohn, Inhomogeneous Electron Gas, *Phys. Rev.* **136**, B864 (1964); W. Kohn and L. J. Sham, Self-Consistent Equations Including Exchange and Correlation Effects, *Phys. Rev.* **140**, A1133 (1965).
- [15] G. Kresse, Ab initio molecular dynamics for liquid metals, *J. Non-Cryst. Solids* **193**, 222 (1995).
- [16] G. Kresse and J. Furthmüller, Efficiency of ab-initio total energy calculations for metals and semiconductors using a plane-wave basis set, *Comput. Mater. Sci.* **6**, 15 (1996).
- [17] G. Kresse and D. Joubert, From ultrasoft pseudopotentials to the projector augmented-wave method, *Phys. Rev. B* **59**, 1758 (1999).
- [18] J. P. Perdew, K. Burke and M. Ernzerhof, Generalized gradient approximation made simple, *Phys. Rev. Lett.* **77**, 3865 (1996).
- [19] S. L. Dudarev, G. A. Botton, S. Y. Savrasov, C. J. Humphreys, and A. P. Sutton, Electron-energy-loss spectra and the structural stability of nickel oxide: An LSDA+U study, *Phys. Rev. B* **57**, 1505 (1998).
- [20] T. Fukui, Y. Hatsugai and H. Suzuki, Chern numbers in discretized Brillouin zone: efficient method of computing (spin) Hall conductances, *J. Phys. Soc. Japan.* **74**, 1674 (2005).
- [21] H. J. Kim, <https://github.com/Infant83/VASPBERRY>, (2018).
- [22] H. J. Kim, C. Li, J. Feng, J.-H. Cho, and Z. Zhang, Competing magnetic orderings and tunable topological states in two-dimensional hexagonal organometallic lattices, *Phys. Rev. B* **93**, 041404(R) (2016).
- [23] S. W. Kim, H. J. Kim, S. Cheon and T. H. Kim, Circular dichroism of emergent chiral stacking orders in quasi-one-dimensional charge density waves, *Phys. Rev. Lett.* **128**, 046401 (2022).
- [24] H. J. Zhao, X. Liu, Y. Wang, Y. Yang, L. Bellaiche and Y. Ma, Zeeman Effect in Centrosymmetric Antiferromagnetic Semiconductors Controlled by an Electric Field, *Phys. Rev. Lett.* **129**, 187602 (2022).
- [25] S. Sattar, M. F. Islam and C. M. Canali, Monolayer MnX and Janus XMnY (X,Y=S, Se, Te): A family of two-dimensional antiferromagnetic semiconductors, *Phys. Rev. B* **106**, 085410 (2022).
- [26] See Supplemental Material at [] for the related energy band structures and MAE vs E .
- [27] R. W. Zhang, C. X. Cui, R. Z. Li, J. Y. Duan, L. Li, Z. M. Yu and Y. G. Yao, Predictable gate-field control of spin in altermagnets with spin-layer coupling, *Phys. Rev. Lett.* **133**, 056401 (2024).
- [28] B. I. Weintrub, Y. L. Hsieh, S. Kovalchuk, J. N. Kirchof, K. Greben, and K. I. Bolotin, Generating intense electric fields in 2D materials by dual ionic gating, *Nat. Commun.* **13**, 6601 (2022).
- [29] L. Han, X. Fu, R. Peng et al., Electrical 180° switching of Néel vector in spin-splitting antiferromagnet, *Sci. Adv.* **10**, eadn0479 (2024).
- [30] D. Xiao, M. C. Chang and Q. Niu, Berry phase effects on electronic properties, *Rev. Mod. Phys.* **82**, 1959 (2010).
- [31] W. Y. Tong, S. J. Gong, X. Wan and C. G. Duan, Concepts of ferrovalley material and anomalous valley Hall effect, *Nat. Commun.* **7**, 13612 (2016).